Supporting Information

Effects of Defects on Photocatalytic Activity of Hydrogen-Treated Titanium Oxide Nanobelts

Scott. K. Cushing,[a,b] Fanke Meng, [a] Junying Zhang,[c] Bangfu Ding,[c] Chih Kai Chen,[d] Chih-Jung Chen,[d] Ru-Shi Liu,[d,e,*] Alan D. Bristow,[b] Joeseph Bright,[a] Peng Zheng, [a] Nianqiang Wu[a,*]

[a]*Department of Mechanical and Aerospace Engineering, West Virginia University, Morgantown, WV 26506-6106,USA*

[b]*Department of Physics and Astronomy, West Virginia University, Morgantown, WV 26506-6315,USA*

[c] *Department of Physics, Beihang University, Beijing 100191, China*

[d] *Department of Chemistry, National Taiwan University, Taipei 106, Taiwan*

[e] *Department of Mechanical Engineering and Graduate Institute of Manufacturing Technology, National Taipei University of Technology, Taipei 106, Taiwan*

*Corresponding authors: TEL: +1-(304)-293-3326, FAX: +1-(304)-293-6689, E-Mails: nick.wu@mail.wvu.edu for (NW); TEL: +886-(2)-33668671, FAX: +886-(2)-33668671, rsliu@ntu.edu.tw (for RSL)

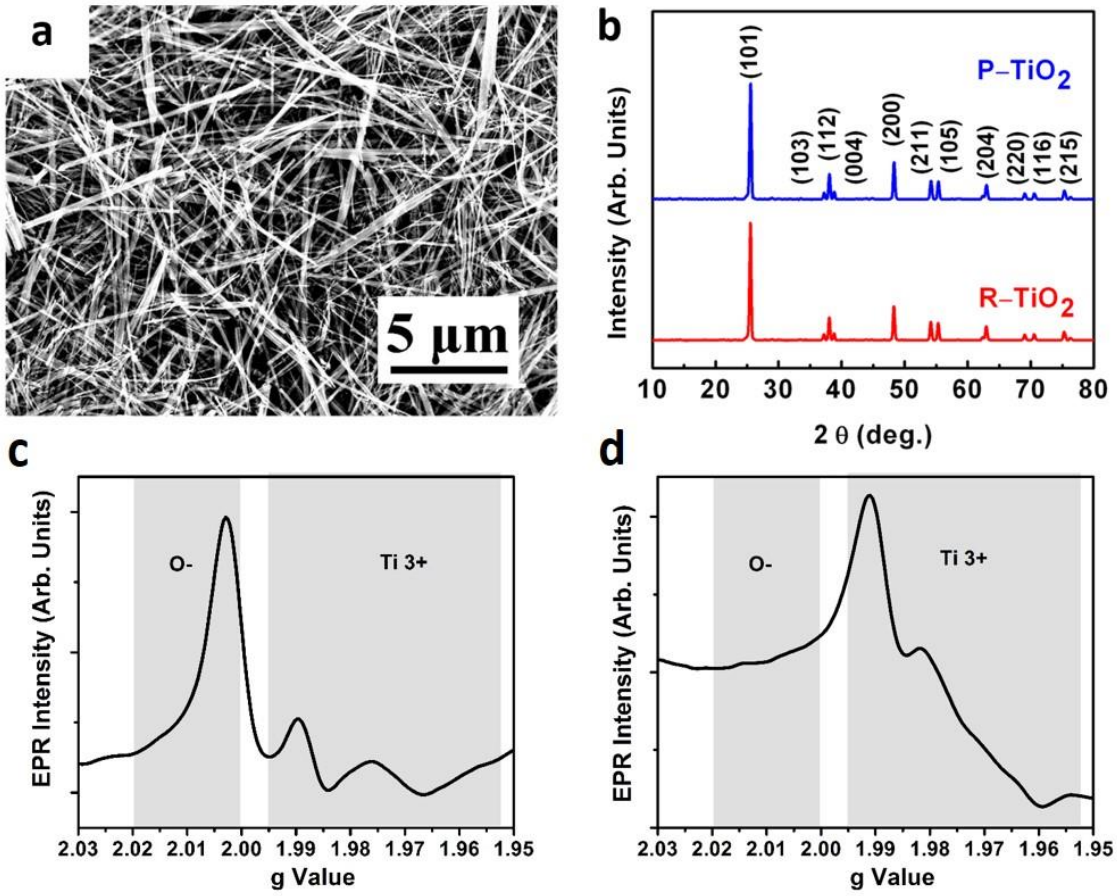

Figure S1. Characterization of TiO_2 nanobelts. (**a)** SEM image of hydrogen-treated TiO_2 nanobelts. (**b**) XRD patterns for the pristine and reduced TiO_2. EPR spectrum for (**c**) pristine and (**d**) hydrogen-treated TiO_2 including the g-value range from Reference 46 and 47 showing the location of the O- surface oxygen vacancy and bulk Ti^{3+} sites.

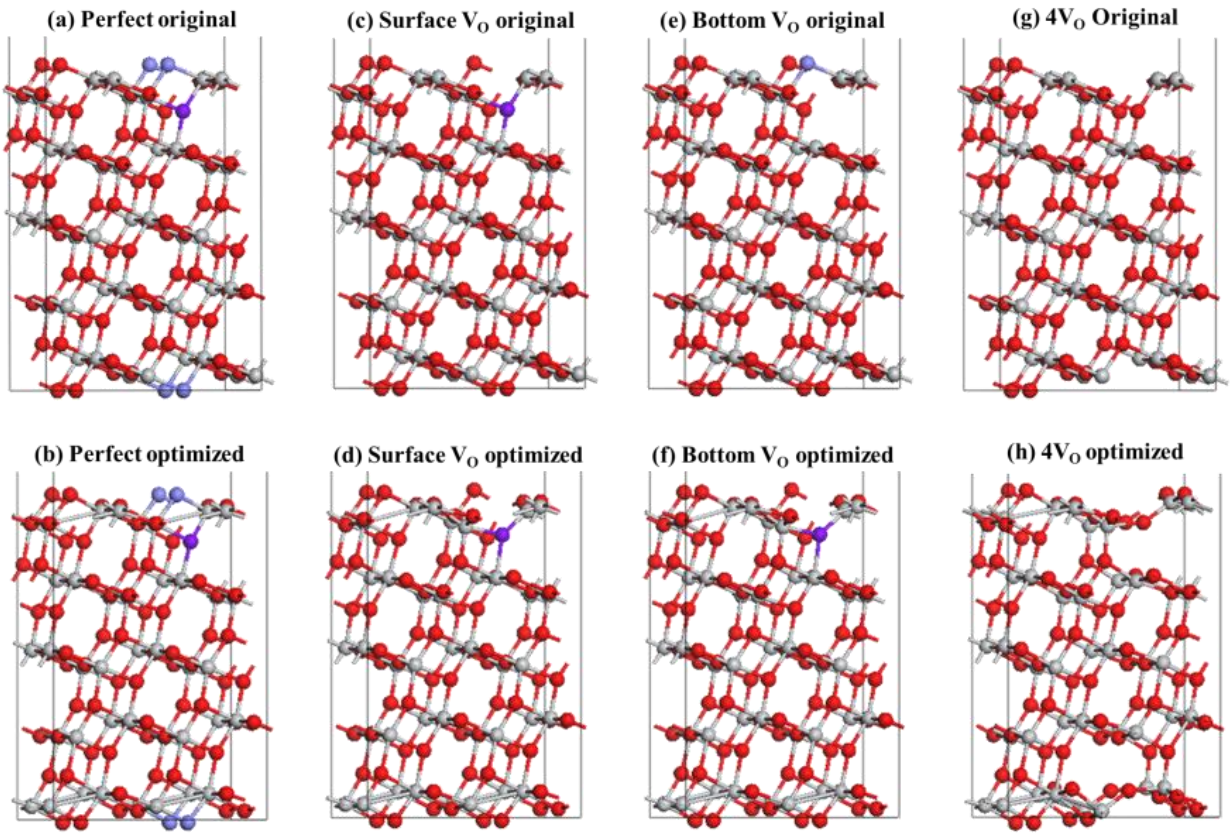

Figure S2. Inclusion of oxygen vacancies in DFT calculation. (a) Position of vacancies in TiO_2 nanobelt, **(b)** optimized TiO_2 nanobelt, **(c)** original, and **(d)** optimized TiO_2 nanobelt with an oxygen vacancy on the surface, (e) original and optimized TiO_2 nanobelt with an oxygen vacancy on the bottom of the surface layer, **(g)** original, and **(h)** optimized TiO_2 nanobelt with four surface vacancies.

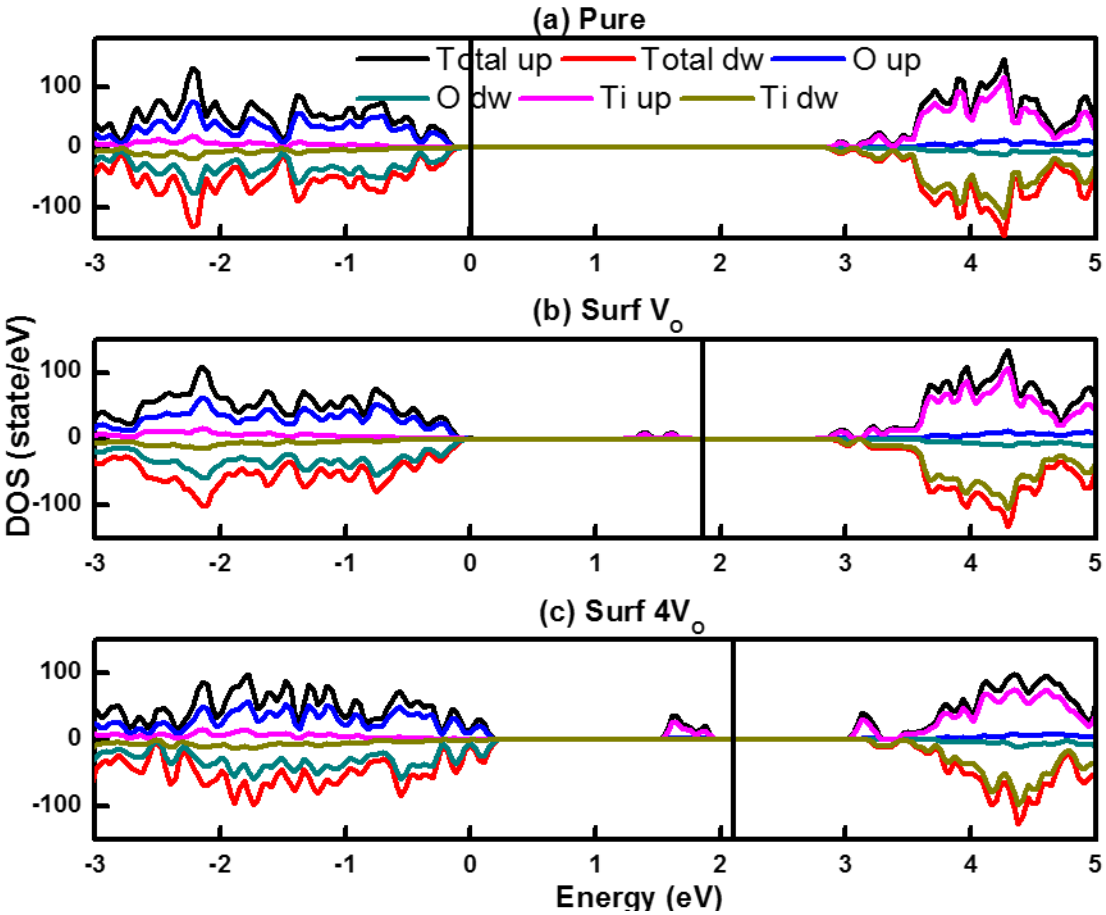

Figure S3. Total and partial density of states from GGA+U calculation. (**a**) pristine TiO_2 nanobelt, (**b**) TiO_2 nanobelt with one oxygen vacancy on the surface or the bottom of the surface layer, and (**c**) TiO_2 nanobelt with four surface vacancies. The solid line indicates the Fermi level. Unlike in Figure 1 of the main manuscript, the DOS here have not been aligned using the energy of the semicore levels, hence the apparent shift of the VB and CB.

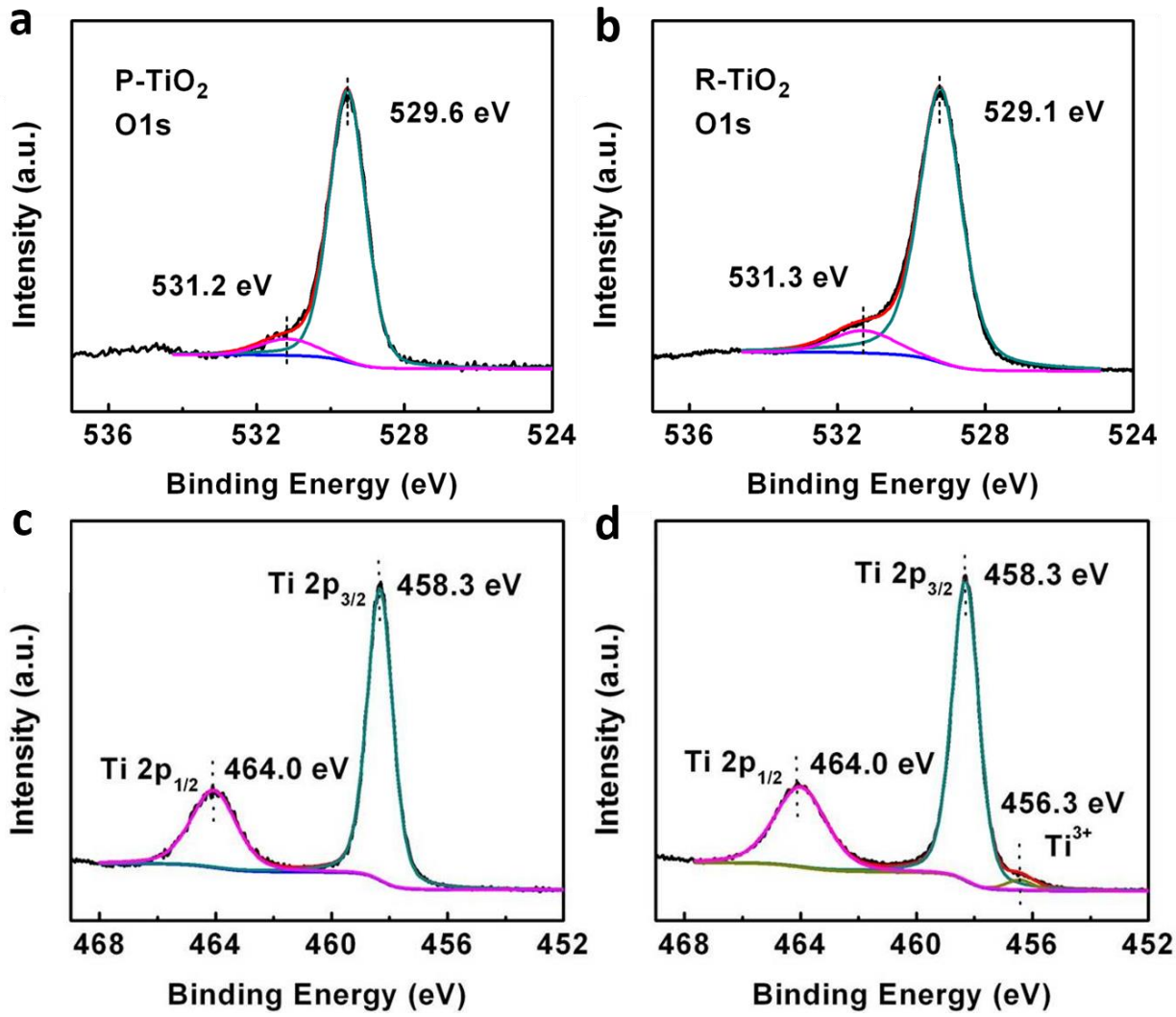

Figure S4. XPS spectra for O *1s* of (**a**) pristine TiO_2 and (**b**) reduced TiO_2. XPS spectra for the Ti *2p* of (**c**) pristine TiO_2 and (**d**) reduced TiO_2. Based on the XPS analysis, the Ti^{3+} content was estimated at 3.4 %, and accordingly the oxygen vacancy content was 0.85 %.

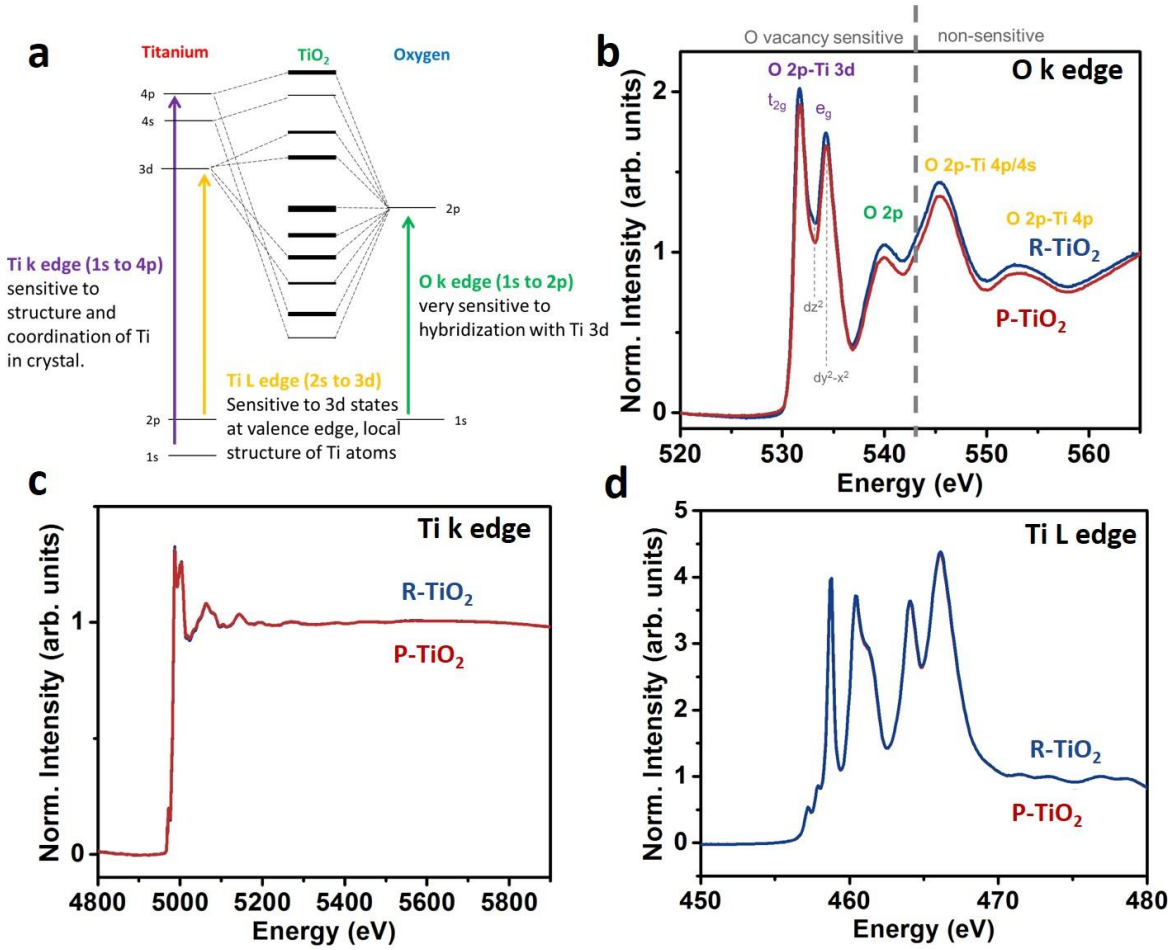

Figure S5. XANES spectra of pristine and reduced TiO_2. (**a**) Explanation of the different XANES transitions and what they are sensitive to, adapted from Ref 41-46. (**b**) O *K* edge with transitions from Reference 41, (**c**) Ti *K* edge, and (**d**) Ti *L* edge.

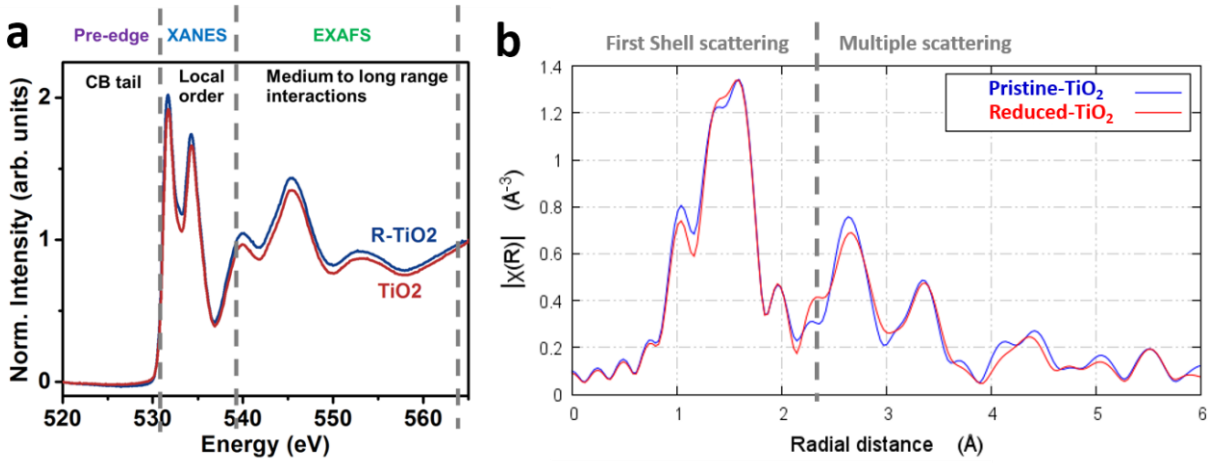

Figure S6. EXAFS for pristine and reduced TiO_2. (**a**) Different regions of the x-ray absorption spectrum and what they are sensitive to. (**b**) EXAFS data showing that to the first shell scattering, and even to multiple scattering, there is little disorder caused by reducing the TiO_2. EXAFS calculated using the ATHENA package: "ATHENA, ARTEMIS, HEPHAESTUS: data analysis for X-ray absorption spectroscopy using IFEFFIT", B. Ravel and M. Newville, J. Synchrotron Rad. 12, pp 537--541 (2005).

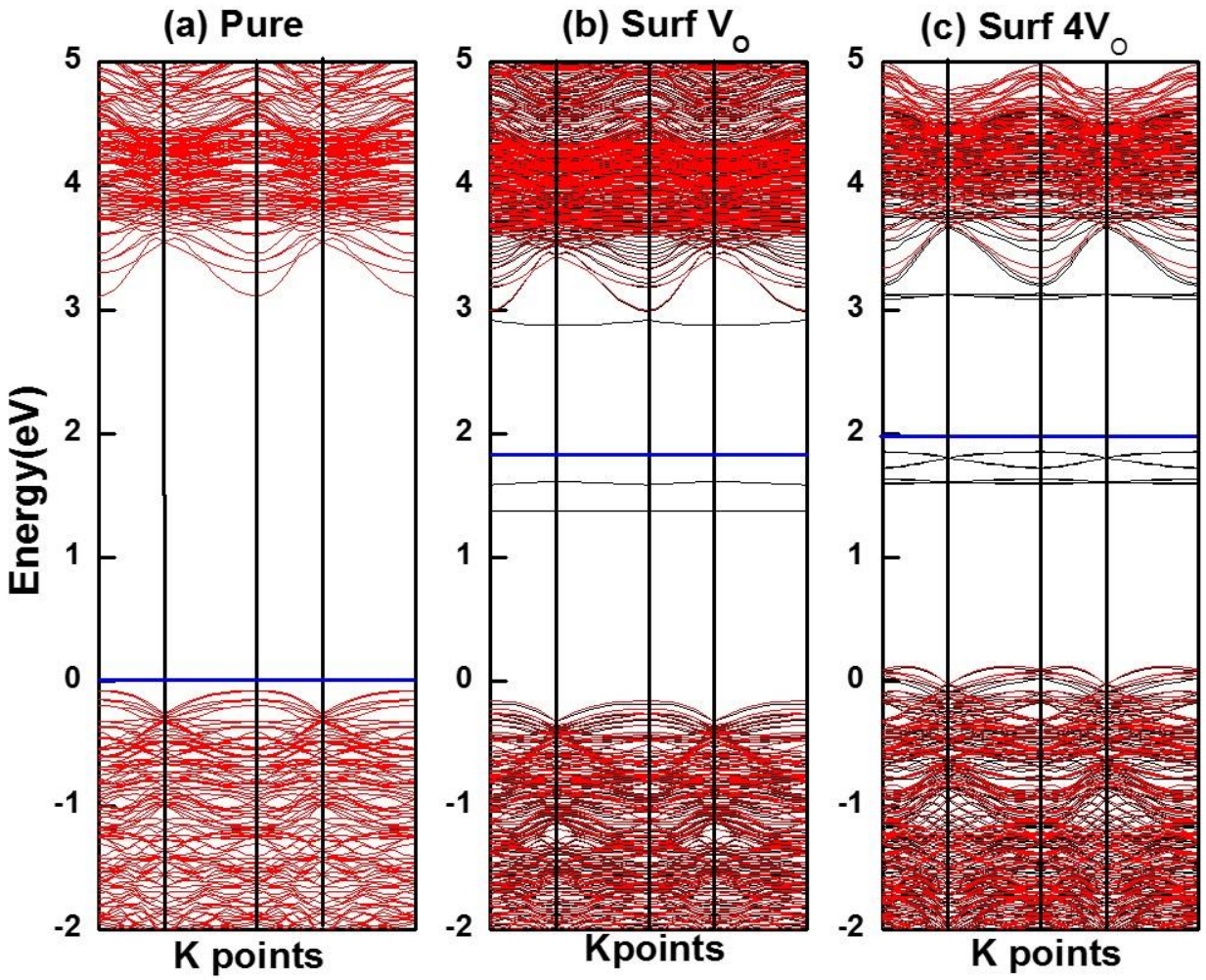

Figure S7. Energy band structures from GGA+U calculation. (**a**) pristine TiO_2 nanobelt, (**b**) TiO_2 nanobelt with one oxygen vacancy on the surface or the bottom of the surface layer, and (**c**) TiO_2 nanobelt with four surface vacancies. The blue lines denoted Fermi energy levels. Unlike in Figure 1 of the main manuscript, the DOS here have not been aligned using the energy of the semicore levels, hence the apparent shift of the VB and CB.

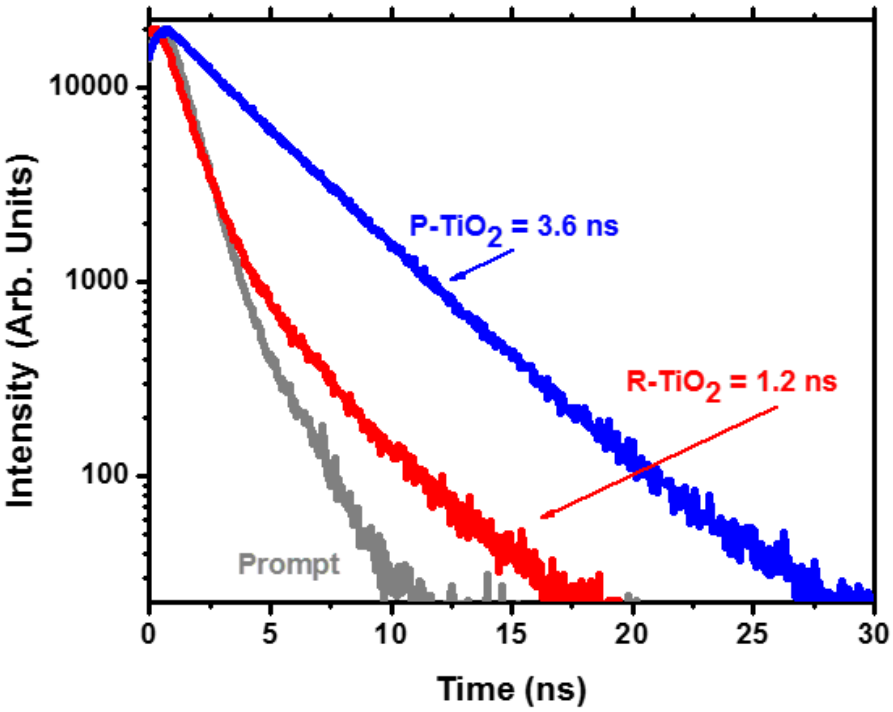

Figure S8. Time-resolved fluorescence for pristine and reduced TiO_2 under excitation at 325 nm. The lifetime is fit by convolution with the instrument response function shown in grey.

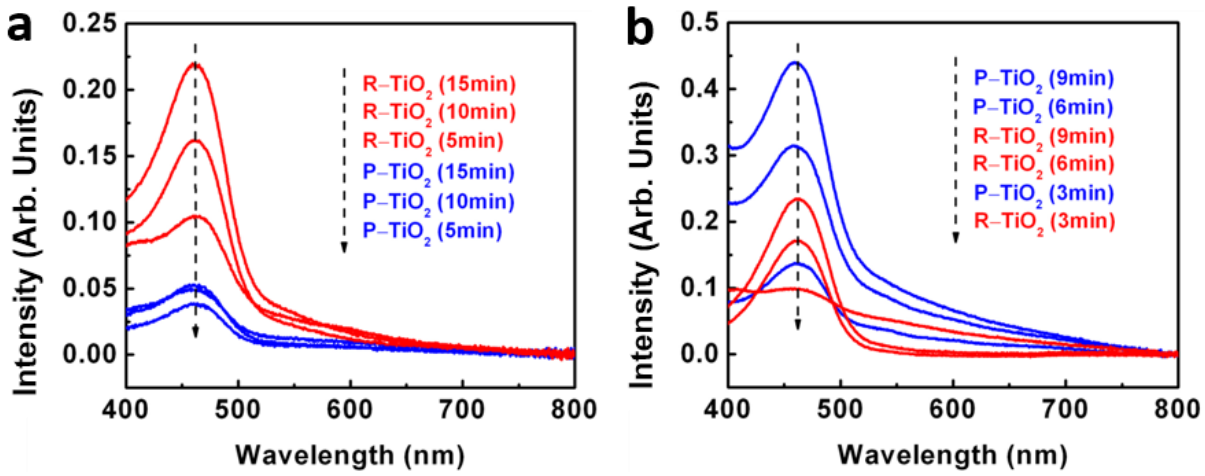

Figure S9. Absorption spectra of NBD-Cl solutions with TiO_2 nanobelts after radiation for different times in (**a**) visible-light and in (**b**) UV light for monitoring superoxide radicals ($O_2^{\bullet -}$).

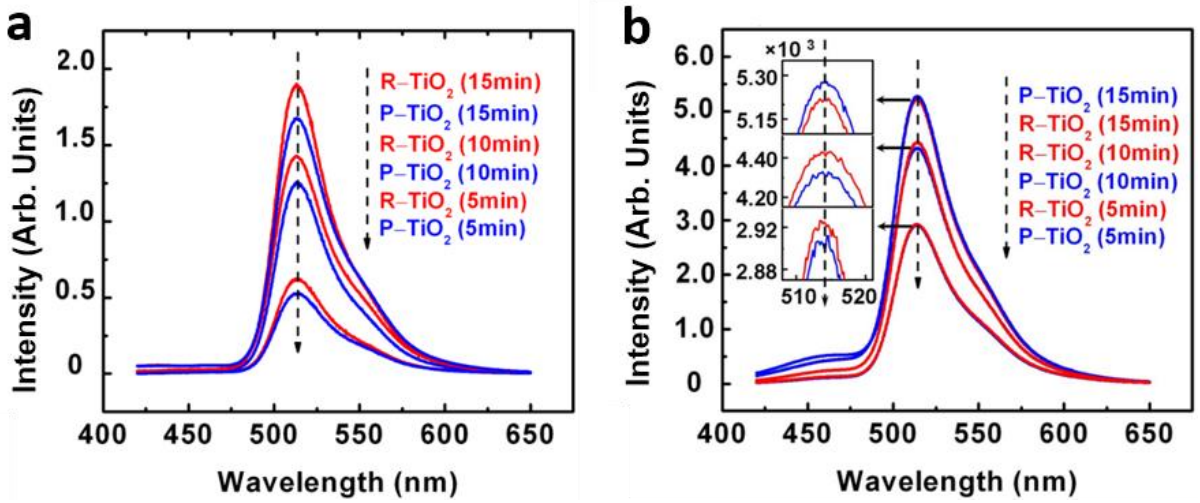

Figure S10. Emission spectra of HPF solution with TiO_2 nanobelts after radiation for different times in (**a**) visible-light, and in **(b**) UV light for monitoring hydroxyl radicals (•OH).